A QUASI-3D NEARSHORE CURRENT MODEL IN WAVE-CURRENT COEXISTING FIELD

Ahmed KHALED SEIF[1,2], Masamitsu KUROIWA[1], Hajime MASE[3], Yuhei MATSUBARA[1], and Mazen ABUALTAYEF[1]

[1]Department of Civil Engineering, Tottori University, Tottori, 680-8552, Japan
[2]National Water Research Center, Fum Ismailiya Canal, P.O. Box 74, Shobra El-Kheima 13411, Cairo, Egypt
[3]Disaster Prevention Research Institute, Kyoto University, Gokasho, Uji, Kyoto 611-0011, Japan

本研究では，波と流れの相互干渉を考慮した準3次元海浜流モデルを開発した．波浪場は流れとの相互干渉，回折の影響を考慮した多方向不規則波の波作用方程式を用いた．流れ場は準3次元海浜流モデルを用い，さらに砕波によるサーフェスローラーの影響も考慮した．まず，沿岸流に関する模型実験結果と比較し，モデルの妥当性を検討した．つぎに，リップチャネルを有する潜堤周辺の波浪場，海浜流場に適用し，さらに，離岸堤および突堤周辺の流れ場に適用し，波流れの相互干渉が流れ場に与える影響について検討した．その結果，波・流れの相互干渉を考慮しない場合と比較して，大きく流速分布が異なることが示され，本モデルの有用性が確認された．

Key Words: *Quasi-3D, wave-current interaction, wave action balance equation, surface roller, coastal structures*

1. INTRODUCTION

An accurate prediction of waves and nearshore currents is a key role in solving coastal engineering problems, especially of those related to the beach morphological evolution. In order to predict the beach evolution, the prediction of nearshore current is required. Previously, the nearshore current fields have been predicted by using a two dimensional depth-averaged model (2DH model), and quasi three dimensional numerical model (Q-3D model) around coastal structures (e.g. Nishimura et al.[1)], Kuroiwa et al.[2)]). However, the model prediction of current field was not accurate and the major reason is due to that the nearshore waves and current fields were independently determined without considering the wave-current interaction.

The main objective of this study is to develop a reliable hydrodynamic numerical model for nearshore waves and currents around coastal regions. This paper introduces a new hydrodynamic model by taking into account the wave-current interaction and the surface roller.

2. NUMERICAL MODEL

The present model consists of two modules, which are wave module and nearshore current module. The wave and nearshore current fields are dependently determined with the consideration of the wave-current interaction.

(1) Wave module

The wave module is based on the multi-directional random wave model, which is based on the wave action balance equation assoiciated with energy dissipation terms for the wave breaking and wave diffraction[3)]. In this module, the wave-current interaction was calculated. The governing wave action balance equation with the wave diffraction effects is

$$\frac{\partial\left(C_x N\right)}{\partial x}+\frac{\partial\left(C_y N\right)}{\partial y}+\frac{\partial\left(C_\theta N\right)}{\partial \theta}= \frac{\kappa}{2\sigma}\left\{\left(CC_g\cos^2\theta N_y\right)_y-\frac{1}{2}CC_g\cos^2\theta N_{yy}\right\}-\varepsilon_b N \quad (1)$$

where N is the wave action density, defined as the wave energy density divided by the angular frequency σ relative to the current (Doppler shift). The horizontal coordinates are x and y, and θ is

the wave direction measured counterclockwise from the x-axis. As suggested by Mase et al.[4], a default value of K=2.5 was used for the diffraction intensity parameter. C and C_g are the wave celerity and group velocity. The characteristic wave velocities with respect to x, y and θ coordinates are accordingly C_x, C_y and C_θ and they defined as

$$C_x = C_g\cos\theta + \tilde{U} \tag{2}$$

$$C_y = C_g\sin\theta + \tilde{V} \tag{3}$$

$$C_\theta = \frac{\sigma}{\sinh 2kh}\left(\sin\theta\frac{\partial h}{\partial x} - \cos\theta\frac{\partial h}{\partial y}\right) + \cos\theta\sin\theta\frac{\partial \tilde{U}}{\partial x} - \cos^2\frac{\partial \tilde{U}}{\partial y} + sin^2\theta\frac{\partial \tilde{V}}{\partial x} - \sin\theta\cos\theta\frac{\partial \tilde{V}}{\partial y} \tag{4}$$

where $\tilde{U}$ and $\tilde{V}$ are the depth-averaged steady currents in the x and y direction, and k is the wave number. The relationships between the relative angular frequency σ, the absolute angular frequency ω, the wave number vector $\mathbf{k}$, the current velocity vector $\tilde{U}$, and the water depth h are shown in the following equations

$$\sigma^2 = g|\mathbf{k}|\tanh|\mathbf{k}|h \tag{5}$$

$$\sigma = \omega - \mathbf{k}\bullet\tilde{\mathbf{U}} \tag{6}$$

In Eq.(1), the parameterized function ε_b describes the mean energy dissipation rate per unit horizontal area due to the wave breaking. The importance of this function was examined for four wave breaking formula by Zheng et al.[5]. In this study, the parameterized wave breaking function for wave energy dissipation was calculated from the following expression for bulk energy dissipation with the ambient current, which proposed by Chawla and Kirby[6].

$$\langle D\rangle = \frac{3\lambda\rho}{32\sqrt{\pi}}\sqrt{\frac{(g\bar{k})^3}{\gamma\tanh\bar{k}h}}\left(\frac{\bar{k}}{\gamma\tanh\bar{k}h}\right)^2 \times H_{rms}^5\left[1-\left\{1+\left(\frac{\bar{k}H_{rms}}{\gamma\tanh\bar{k}h}\right)^2\right\}^{-5/2}\right] \tag{7}$$

where $\langle D\rangle$ is the bulk energy dissipation by all breaking waves, H_{rms} is the root-mean-square wave height, and $\bar{k}$ is the wave number corresponding to the mean angular frequency $\bar{\sigma}$, and the scaling parameters λ and γ are set to 0.4 and 0.6, respectively.

The wave breaking energy dissipation coefficient ε_b is calculated as

$$\varepsilon_b = \langle D\rangle \Big/ \left(0.125\rho g H_{rms}^2\right)\bar{\sigma} \tag{8}$$

Furthermore, the energy balance equation was used in association with the surface roller term, which is based on the quation of Dally and Brown[7], as follows

$$-D_b + \frac{\partial}{\partial x}\left(\frac{1}{2}MC_r^2\cos^2\bar{\theta}\right) + \frac{\partial}{\partial y}\left(\frac{1}{2}MC_r^2\sin^2\bar{\theta}\right) = -g\beta_D M \tag{9}$$

where D_b is the wave breaking energy dissipation, M is the wave-period-averaged mass flux, C_r is the roller speed ($\approx C$), and the roller dissipation coefficient β_D was set to 0.1 The stresses due to the rollers are determined as follows

$$R_{xx} = MC_r\cos^2\bar{\theta} \tag{10}$$

$$R_{yy} = MC_r\sin^2\bar{\theta} \tag{11}$$

$$R_{xy} = R_{yx} = MC_r\sin 2\bar{\theta} \tag{12}$$

(2) Nearshore current module

The nearshore current module is based on the Q-3D nearshore current model, which was proposed by Kuroiwa et al.[2]. The governing equations are defined as follows

$$\frac{\partial U}{\partial t} + U\frac{\partial U}{\partial x} + V\frac{\partial U}{\partial y} + W\frac{\partial U}{\partial z} = -g\frac{\partial \bar{\zeta}}{\partial x} - \frac{\partial(S_{xx}+R_{xx})}{\partial x} - \frac{\partial(S_{xy}+R_{xy})}{\partial y} + \frac{\partial}{\partial x}\left(\nu_h\frac{\partial U}{\partial x}\right) + \frac{\partial}{\partial y}\left(\nu_h\frac{\partial U}{\partial y}\right) + \frac{\partial}{\partial z}\left(\nu_v\frac{\partial U}{\partial z}\right) \tag{13}$$

$$\frac{\partial V}{\partial t} + U\frac{\partial V}{\partial x} + V\frac{\partial V}{\partial y} + W\frac{\partial V}{\partial z} = -g\frac{\partial \bar{\zeta}}{\partial y} - \frac{\partial(S_{yx}+R_{yx})}{\partial x} - \frac{\partial(S_{yy}+R_{yy})}{\partial y} + \frac{\partial}{\partial x}\left(\nu_h\frac{\partial V}{\partial x}\right) + \frac{\partial}{\partial y}\left(\nu_h\frac{\partial V}{\partial y}\right) + \frac{\partial}{\partial z}\left(\nu_v\frac{\partial V}{\partial z}\right) \tag{14}$$

where U, V and W are the steady current velocities in the x, y and z directions. S_{xx}, S_{yy}, S_{xy}, S_{yx}, and S_{yy} represent the terms of excess momentum fluxes due to the waves. ν_v represents the turbulent eddy viscosity coefficients in the vertical direction estimated by Tsuchiya et al.[8], and ν_h represents the turbulent eddy viscosity coefficients in the horizontal direction estimated by Larson et al.[9]. The radiation stress part was modified by adding the momentum fluxes term due to the surface roller as R_{xx}, R_{yy}, R_{xy}, R_{yx}, and R_{yy}. The continuity equation is expressed as

$$\frac{\partial U}{\partial x} + \frac{\partial V}{\partial y} + \frac{\partial W}{\partial z} = 0 \tag{15}$$

The depth-integrated continuity equation is

$$\frac{\partial \bar{\zeta}}{\partial t} + \frac{\partial \tilde{U}(h+\bar{\zeta})}{\partial x} + \frac{\partial \tilde{V}(h+\bar{\zeta})}{\partial y} = 0 \tag{16}$$

where $\tilde{U}$ and $\tilde{V}$ are the depth-averaged steady currents, and $\bar{\zeta}$ is the mean water level.

An iterative feed back process between the wave module and the nearshore current module was

carried out to obtain the steady state condition, as shown in **Fig.1**. In this study, in order to reach to the steady state condition, the wave field calculation was updated at each iteration by taking the average wave field between the previous and present iteration to compute the nearshore current field for the next iteration.

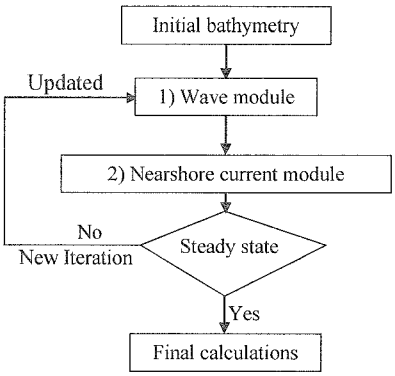

Fig.1 Flowchart of the numerical model.

3. MODEL TESTS

Several model tests were carried out, Large-Scale Sediment Transport Facility (LSTF) experimental test perforemd by Hamilton and Ebersole[10], and numerical model tests, without aiming for formal verification, but immediately showing the new proposed models capabilities. The models setups are shown below and the results are addressed in section 4.

(1) LSTF experimental model test setup

The present model was applied to the longshore current experimetal model under an irrigular wave from the laboratory experiments data of LSTF, to calibrate the waves and nearshore current fields. The computation was performed in a concrete beach with alongeshore dimension of 31m and a cross-shore dimension of 21m, and the plane slope was 1:30. The grid size was $\Delta x=\Delta y=0.5$m. The significant wave height at the offshore boundary was 0.667m, the significant wave period was 2.5s, and the wave direction at the wave generations was 10 degree. In Eq.7, λ was set to 1.8 in order to calibrate the nearshore current field.

(2) Numerical model tests setup

Three model tests associated with rip-channel between two submerged breakwaters, groins and detached breakwaters were carried out under field scale. The compuatation conditions for the model tests are shown in Table 1. The width of rip channel was 70m. The distance between the groins was 400m. The breakwater away from the shoreline of 150m.

Table 1 Computation conditions of model tests

Parameters	Model test		
	Submerged breakwater	Groins	Detached breakwater
Area along x cross, km	1.0 x 0.6	0.8 x 0.5	0.6 x 0.6
Length, m	200.0	250.0	200.0
Slope	1/50	1/50	1/50
Grid size $\Delta x=\Delta y$, m	10.0	10.0	10.0
H_s, m	1.5	1.5	1.5
T_s, s	7.0	7.0	7.0
θ_s, degree	0.0	20.0	0.0

4. RESULTS AND DISSCUSSION

(1) LSTF experimental test results

The computed results of our model were compared against the experiemntal model results. **Figs.2(a)** and **(b)** show comparisons between the computed and measured wave height distribution, and longeshore current, with and without the wave-current interaction and the surface roller effect. The model was running until the steady state with the consideration of wave-current interaction was reached. The prediction significant wave height was in a good agreement when the wave-current interaction was considered, as shown in **Fig.2(a)**. The computed results of longshore currents with the effect of the surface roller was not only shifted the peak toward the shoreline, but also increased the maximum current magnitudes in the surf zone, as shown in **Fig.2(b)**. From these results, it was found that the computed wave height distribution and longeshore current were in a good agreement with the experiemental results.

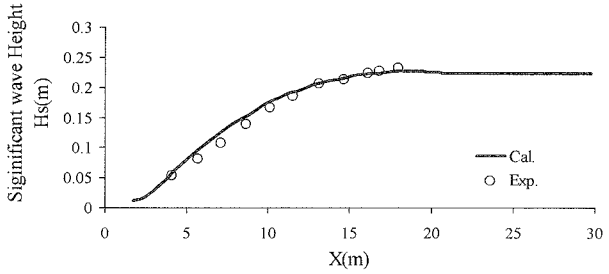

Fig.2(a) Computed and observed wave height distribution.

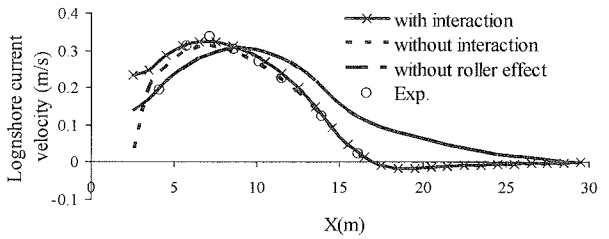

Fig.2(b) Computed and observed longshore current velocities.

(2) Numerical tests results

a) Submerged breakwaters test results

The computed results of model test asscociated with the rip-channel between two submerged breakwaters are shown in **Fig.3** and **Fig.4**. The effects of considering the interaction or not on the significant wave height distribution are shown in **Fig.3(a)** and **Fig.3(b)**. **Figs.3(c)** and **(d)** show comparisons between the computed cross-shore wave height distribution with and without the interaction at y=350 (reef crown) and y=500m (rip-channel), respectively.

The wave height at rip-channel was increased due to the rip-current. On the other hand, the wave height at the reef crown was decreased due to the strong shoreward current. Whereas the model was run three feed backs between the wave and the nearshore current fields till the steady state was achieved.

Comparisons between the computed depth-averaged current velocity with and without the interaction are shown in **Fig.4(a)** and **Fig.4(b)**. The computed surface and bottom current velocities with the interaction are shown in **Fig.4(c)** and **Fig. 4(d)**. **Fig. 4(e)** and **Fig. 4(f)** show comparisons between the computed depth-averaged current velocities $\tilde{U}$, $\tilde{V}$ with and without the interaction at y=500m and x=350m, respectively.

It was found that by considering the wave-current interaction, the magunitude and direction of the current velocities were changed. Furthermore, the model can compute the wave and nearshore current in the steady state.

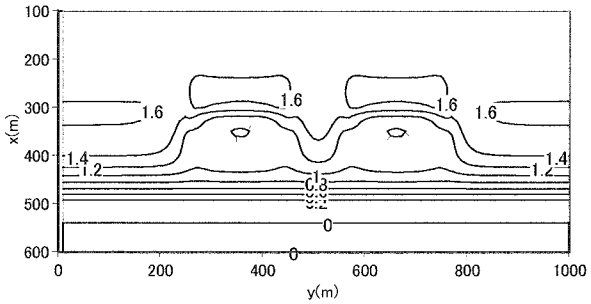

Fig.3(a) Computed wave height distribution without interaction.

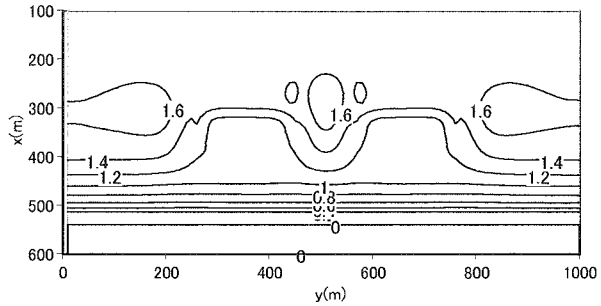

Fig.3(b) Computed wave height distribution with interaction.

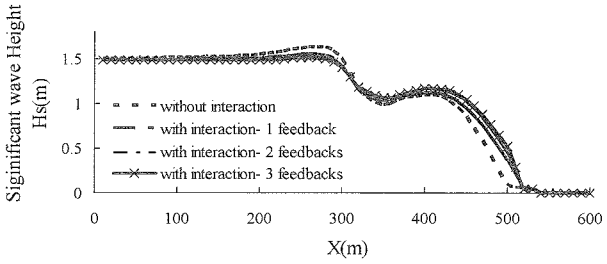

Fig.3(c) Computed cross-shore wave height distribution (y=350m).

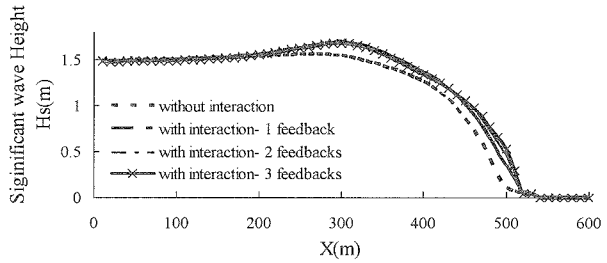

Fig.3(d) Computed cross-shore wave height distribution (y=500m).

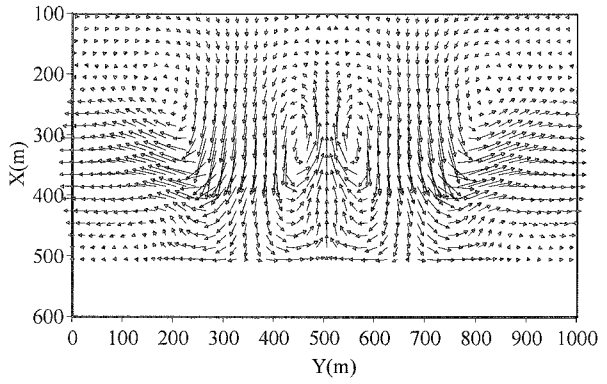

Fig.4(a) Computed depth-averaged current without interaction.

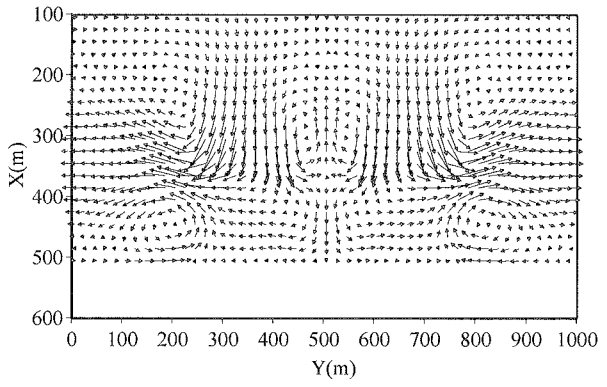

Fig.4(b) Computed depth-averaged current with interaction.

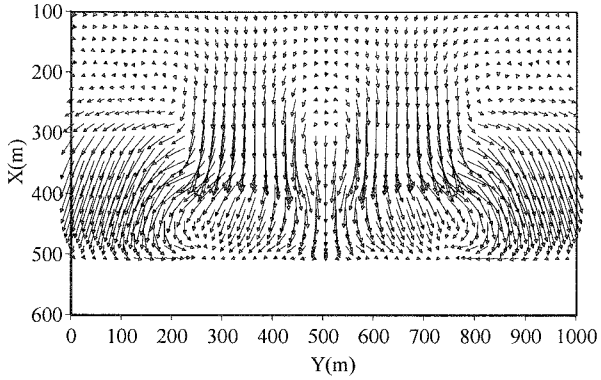

Fig.4(c) Computed surface current velocity with interaction.

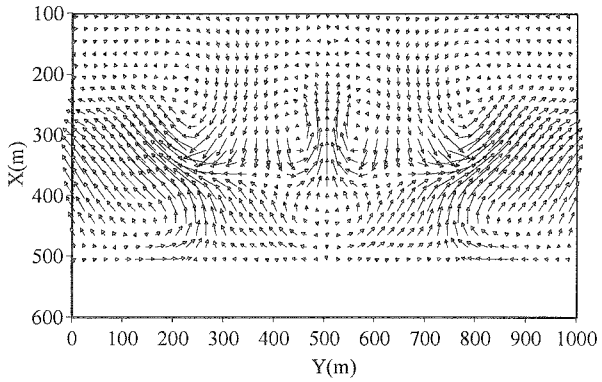

Fig.4(d) Computed bottom current velocity with interaction.

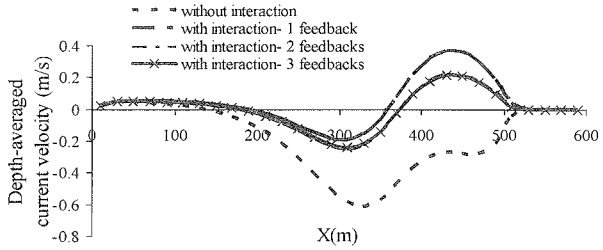

Fig.4(e) Computed depth-averaged longshore current velocity, $\tilde{U}$ (y=500m).

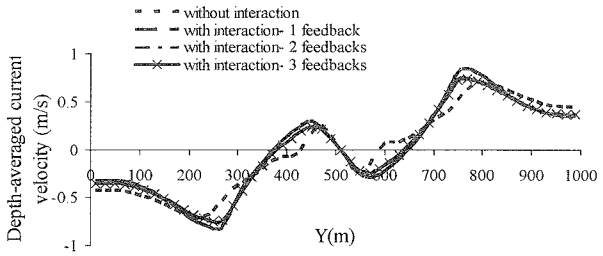

Fig.4(f) Computed depth-averaged cross-shore current velocity, $\tilde{V}$ (x=350m).

b) Groins model test results

The computed results of model test asscociated with two groins are seen in **Fig.5** and **Fig.6**. The computed significant wave height distribution with and without the interaction are compared in **Fig.5(a)** and **Fig.5(b)**. **Fig.6(a)** shows the computed bottom current velocity with the interaction, and **Fig.6(b)** shows the comparisons between the computed depth-averaged current velocity $\tilde{V}$ with and without the interaction at x=350m.

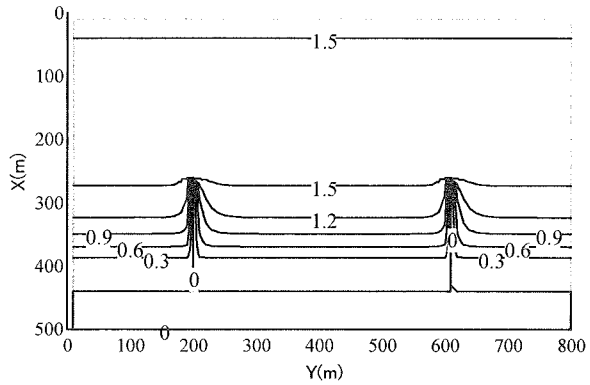

Fig.5(a) Computed wave height distribution without interaction.

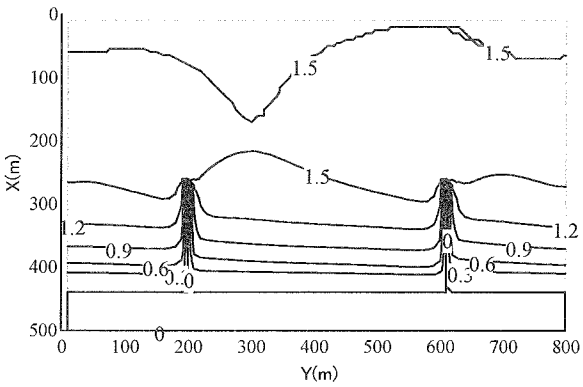

Fig.5(b) Computed wave height distribution with interaction

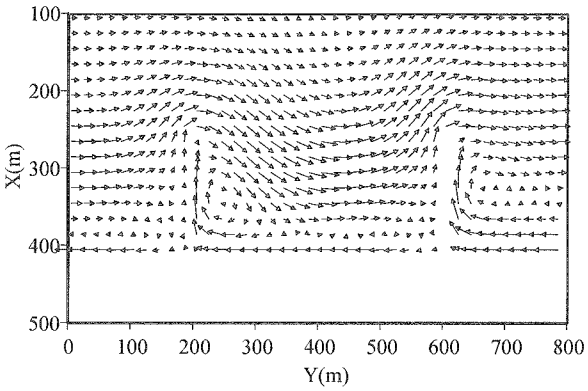

Fig.6(a) Computed bottom current velocity with interaction

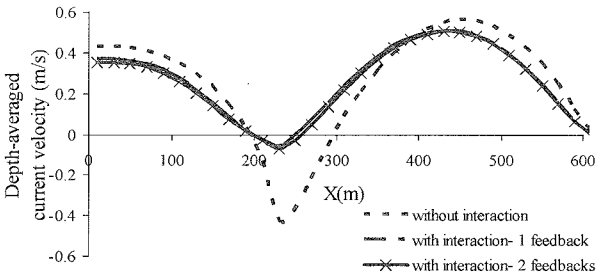

Fig.6(b) Computed depth-averaged cross-shore current velocity, $\tilde{V}$ (x=350m).

As a conclusion, the wave height distribution with the current consideration in the computation, the model was reached the steady state after two feed backs. The magunitude and direction of the current velocities between the groins were changed due to the wave-current interaction.

c) Detached breakwater model test results

The computed results of model test asscociated with detached breakwater are seen in **Fig.7** and **Fig.8**. The model results of the significant wave height distribution with and without the consideration of wave-current interaction are shown in **Fig.7(a)** and **Fig.7(b)**. **Fig.8(a)** shows the computed bottom current velocity with interaction. **Fig.8(b)** shows the computed depth-averaged current velocity $\tilde{V}$ at x=450m with/without the

interaction. By considering the wave-current interaction, it was found that the wave height distribution behind the detached breakwater was changed, and the magunitude and direction of the current velocities were changed.

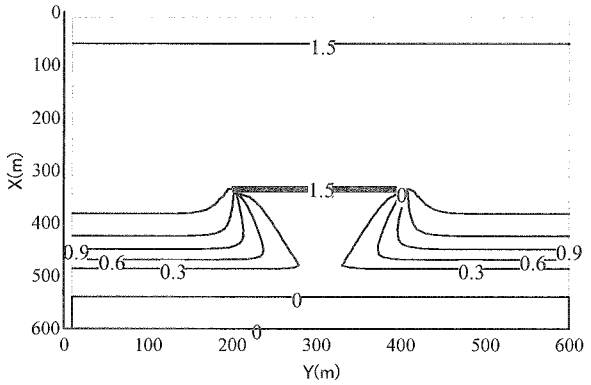

Fig.7(a) Computed wave height distribution without interaction.

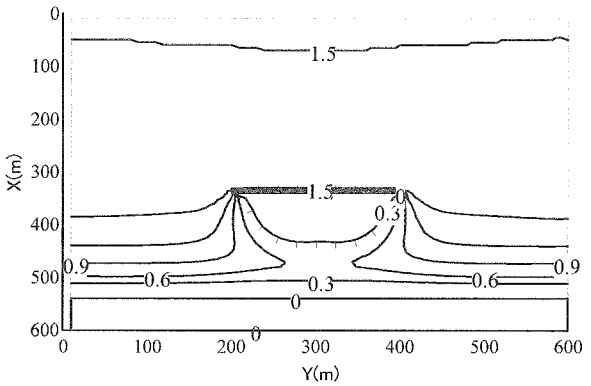

Fig.7(b) Computed wave height distribution with interaction.

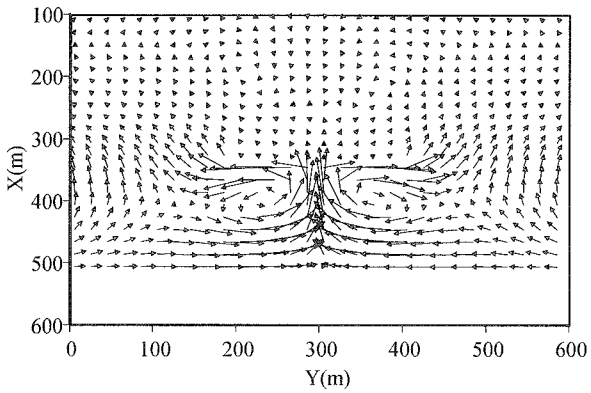

Fig.8(a) Computed bottom current velocity with interaction.

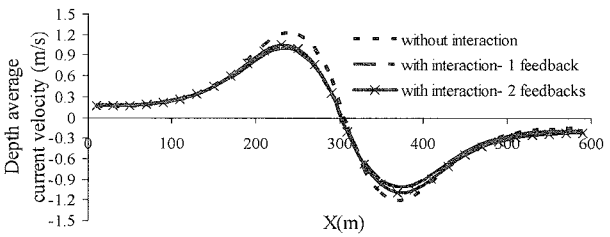

Fig.8(b) Computed depth-averaged cross-shore current velocity, $\tilde{V}$ (x=450m).

5. CONCLUSION

In this article, the hydrodynamic of nearshore waves and currents around coastal structures was described. The applicability of the model was demostrated through several numerical tests and compared against experimental results. The new proposed hydrodynamic numerical model shows good agreement with the experimental results. Furthermore, it was found that the wave-current interaction with the surface roller was significantly playing an important role for the prediction of the 3D hydrodynamics computation.

As a future work, applications using the field observation are required to help and strengthen the utility of this model.

REFERENCES

1) Nishimura, H. *Computation of nearshore current, nearshore dynamics and coastal process -Theory, Measurements and Predictive Models*, University of Tokyo Press, pp.271-291, 1988.

2) Kuroiwa, M. , Matsubara, Y. , Kuchiishi, T., Kato, K., Noda, H., and Son, C.B. A morphodynamic model based on Q-3D nearshore current model and application to barred beach, *28th ICCE*, pp.3409-3421, 2002.

3) Mase, H., Yuhi, M., Amamori, H., and Takayama, T. Phase Averaging wave prediction model with breaking and diffraction effects in wave-current coexisting field, *Annual Journal of Coastal Engineering*, JSCE., 51, No.1, pp.6-10, 2004. (In Japanese)

4) Mase, H. Multi-directional random wave transformation model based on energy balance equation, *Coastal Eng J.*, 43, No.4, pp.317-337, 2001.

5) Zheng, J., Mase, H., Demirbilek, Z., and Lin, Li. Implementation and evaluation of alternative wave breaking formula in a costal spectral wave model, *Ocean Eng*, 35, pp.1090-1101, 2008.

6) Chawla, A., and Kirby, J.T. Monochromatic and random wave breaking at blocking points. *Journal of Geophysical Research*, 107, No. C7, 2002.

7) Dally, W.R., and Brown, Ch.A. A modeling investigation of the breaking wave roller with application to cross-shore currents1995. *Journal of Geophysical Research*, 100, No. C12, pp.873-883, 2002.

8) Tsuchiya, Y., Yamashita, T., and Uemoto, M. A model of undertow in the surf zone. *Proceedings of the 33rd Japanese Conference on Coastal Engineering*, JSCE, pp.31-35, 1986.

9) Larson, M., and Kraus, N. C. *NMLONG: Numerical model for simulating longshore current.* Coastal and Hydraulics Laboratory Technical Report ERDC/CHL TR-02-22. Vicksburg, MS: U.S. Army Engineer Research and Development Center, 2002.

10) David G. Hamilton and Bruce A. Ebersole, Esablishing uniform longeshore currents in a large-scale sediment transport facility, *Coastal Eng*, 42, pp.199-218, 2001.